Letters in Applied NanoBioScience
Open-Access Journal (ISSN: 2284-6808)

Article
Volume 14, Issue 3, 2025, 132
https://doi.org/10.33263/LIANBS143.132

Synthesis and X-Ray Diffraction Data for Monophosphates Type $Pb_{3-2x}K_xNd_x(PO_4)_2$

Chaimaa Moukhfi [1,*], Youssef Ghandi [1], Marouani Hamza [1], Smail ElMakhloufy [1], Soufiane Zerraf [1], Bouchra Gourja [1], Malika Tridane [1,2], Said Belaaouad [1]

[1] Physical Chemistry of Materials Laboratory, Ben M'Sick Faculty of Science, Hassan II University of Casablanca, Casablanca, Morocco
[2] Regional Center for Management and Training Profession CRMEF, Casablanca, Morocco
* Correspondence: chaimaa.mkf@gmail.com;

Received: 23.01.2024; Accepted: 7.07.2024; Published: 6.09.2025

Abstract: In our research, we focused on synthesizing new monophosphate phases, namely $Pb_{3-2x}K_xNd_x(PO_4)_2$, by varying the parameter x (0.05, 0.10, 0.15, 0.20, 0.25, 0.50, and 0.75). We provided a detailed account of the chemical preparation methods and presented the X-ray diffraction (XRD) results for these phases. Our main goal was to assess the possibility of substituting elements within $B_3(XO_4)_2$ structures akin to $Sr_3(PO_4)_2$. This study was prompted by the absence of previous efforts to explore substitutions within lead phosphate structures. Consequently, we successfully formulated these novel solid solutions, $Pb_{3-2x}K_xNd_x(PO_4)_2$. The phases with x-values of 0.05, 0.10, and 0.15 exhibit the structure of β-$Pb_3(PO_4)_2$, while those with x-values of 0.20, 0.25, 0.50, and 0.75 show a structure similar to that of $Sr_3(PO_4)_2$. The incorporation of K^+ and Nd^{3+} ions in place of Pb^{2+} resulted in a slight volume reduction. This reduction is consistent with the average ionic radii of potassium and neodymium, which are marginally smaller than that of lead.

Keywords: monophosphate; chemical preparation; x-ray diffraction data; substitution; potassium; neodymium.

1. Introduction

Previous works [1-4] have shown the existence of $ABLn(PO_4)_2$ phosphates in which A = K, Rb, Cs, Ba and B =Ca, Sr, H. The structure of these phases, determined on a single crystal of $KCaNd(PO_4)_2$ [5], is derived from the hexagonal variety of $LnPO_4$ by inserting potassium into the large tunnels of the lattice. Calcium and neodymium statistically occupy the lanthanide sites. Since thallium (T^{1+})in oxidation state +1 has an ionic radius close to that of rubidium, we have prepared the new phases $TlCaLn(PO_4)_2$ where Ln = Nd, Sm, Eu, Gd, Dy, and $TlCaBi(PO_4)_2$ [6].

This substitution could result in a modification of the physical properties due to the fact that the Tl+ has a free doublet $6s^2$. On the other hand, several researchers have explored the potential for substituting elements within the $B_3(XO_4)_2$ structures resembling $Sr_3(PO_4)_2$. Consequently, solid solutions with the formula $Sr_{3-2x}Na_xLn_x(PO_4)_2$ (Ln = Nd, Gd) were synthesized, with x varying between 0 and 0.9 for Nd and between 0 and 0.5 for Gd. These solid solutions share the same crystal structure as $Sr_3(PO_4)_2$ [7,8]. A few of these phases display

fascinating optical characteristics [9]. $Pb_3(PO_4)_2$ has two allotropic varieties α$Pb_3(PO_4)_2$ and β $Pb_3(PO_4)_2$.

The structure of α $Pb_3(PO_4)_2$ has an isotype with $Sr_3(PO_4)_2$. The X-ray diffraction reveals that the compound β $Pb_3(PO_4)_2$ crystallizes in the monoclinic system. The shift from the monoclinic form β to the hexagonal form α of $Pb_3(PO_4)_2$ occurs upon heating to 200°C, and this transition is marked by a significant increase in dielectric permittivity. As we are not aware of any substitutions within lead phosphate, we have proposed to do so. The introduction of rare earth ions into the $Pb_3(PO_4)_2$ structure can have the potential to yield materials exhibiting intriguing optical characteristics [10]. As we know, the lead has ferroelastic properties; the new material $Pb_{3-2x}K_xNd_x(PO_4)_2$ could also have interesting ferroelectric properties [11,12], then we synthesized these new phases.

The present work aims to present the synthesis of new phases $Pb_{3-2x}K_xNd_x(PO_4)_2$ with x = 0.05,0.10,0.15,0.20,0.25,0.50 and 0.75 and their crystallographic characterization as well as the study of the progression of parameters aH and cH, along with the volume VH.

2. Materials and Methods

2.1. Starting materials.

Neodymium oxide Nd_2O_3 is one of Merck's 99.9% pure products. It is calcined before use at 800°C for 12 hours.

Lead nitrate $Pb(NO_3)_2$ is dried in an oven at around 150°C because, above this temperature, it oxidizes.

Potassium carbonate K_2CO_3 is air-dried at 150°C for 3 days.

Ammonium monohydrogen monophosphate $(NH_4)_2HPO_4$ dried in an oven at about 50°C.

2.2. Methods of synthesis.

All syntheses are carried out in the solid phase. The starting materials are mixed in stoichiometric ratios, ground, and pelletized at 70-150 Kg/cm^2. They are then carried in alumina baskets at the desired temperature in electric ovens up to 1200°C [13].

The temperature is measured using a Pt-Pt thermocouple. It is automatically regulated by Stanton Redcroft PT 13-type devices.

2.3. Preparatory reaction.

The new material $Pb_{3-2x}K_xNd_x(PO_4)_2$with different x:0.05, 0.10, 0.15, 0.20, 0.25, 0.50 and 0.75were prepared by mixing the necessary starting materials $Pb(NO_3)_2$, K_2CO_3, Nd_2O_3 and $(NH_4)_2HPO_4$according to the following chemical reaction:

$$2(3-2x)Pb(NO_3) + xK_2CO_3 + x\,Nd_2O_3 + 4(NH_4)_2HPO_4 \rightarrow 2Pb_{3-2X}K_XNd_X(PO_4)_2 + xCO_2 + 8NH_3 + 6H_2O + 4(3-2x)NO_2 + (3-2x)O_2 \quad (1)$$

His precisely balanced blend is thoroughly homogenized and subjected to calcination at 400°C for a duration of 12 hours. Subsequently, it is finely ground again, formed into pellets, and subjected to a 4-day treatment at 650°C.

2.4. X-ray diffraction crystallography.

We gathered diffraction data at room temperature using either a Philips "PWW 1700" or a device "CGR θ 60" employing the Bragg-Brentano geometry. The experiments utilized CuKα radiation (λ = 1.54051 Å) with operating conditions set at 40 Kv and 30 mA [14-23]. The experimental 2θ range spanned from 7 to 80° 2θ, employing a step size of 0.01° 2θ, and each step had a counting time of 30 s [24,25].

3. Results and Discussion

3.1. Isotype phases of α $Pb_3(PO4)_2$.

The X-ray diffraction powder patterns for the $Pb_{3-2x}K_xNd_x(PO_4)_2$ phases with x values of x=0.20, 0.25, 0.50, and 0.75 demonstrate structural similarity to the $Sr_3(PO_4)_2$ configuration. The parameters aH and cH are listed together with the volume VH [26,27] in Table 1.

Table 1. Parameters aH and cH and volume VH of materials $Pb_{3-2x}K_xNd_x(PO_4)_2$ for x=0.20; x=0.25; x=0.50 et x=0.75.

Value of x	Phase	(a_H ± 0,01)Å	(c_H ± 0,01)Å	(V_H ± 2)Å^3
0,20	$Pb_{2,60}K_{0,20}Nd_{0,20}(PO_4)_2$	5,51	20,33	534
0,25	$Pb_{2,50}$ $K_{0,25}Nd_{0,25}PO_4)_2$	5,51	20,35	535
0,50	$Pb_{2,00}K_{0,50}Nd_{0,50}(PO_4)_2$	5,50	20,43	535
0,75	$Pb_{1,50}K_{0,75}Nd_{0,75}(PO_4)_2$	5,47	20,44	530

It can be seen that the threshold value ofx, referred to asx1, for reaching the solid solution is close to 0.75. Beyond this point, particularly when x equals 1, the X-ray diffraction powder patterns reveal the presence of the boundary phase $Pb_{1.5}K_{0.75}Nd_{0.75}(PO_4)_2$, along with the phases $K_3Nd(PO_4)_2$ and $NdPO_4$.When x exceeds 0.75, the formation of the limit composition $Pb_{1.5}K_{0.75}Nd_{0.75}(PO_4)_2$ can be conceptualized as follows:

$$1.5Pb_{3-2X}K_XNd_X(PO_4)_2 + {}^3\!/_4\,xCO_2 + 6NH_3 + {}^9\!/_2\,H_2O + 3(3-2x)NO_2 + ({}^9\!/_2 - {}^3\!/_4\,x)O_2$$

$$1.5(3-2x)Pb(NO_3)_2 + {}^3\!/_4\,xK_2CO_3 + {}^3\!/_4\,xNb_2O_3 + 3(NH_4)_2HPO_4 \rightarrow (3-2x)Pb_{1.5X}K_{0.75}Nd_{0.75}(PO_4)_2 + (x-0.75)K_3Nd(PO_4)_2 + 2(x-0.75)NdPO_4$$

Figure 1 shows the development of the parameters of the parameters a_H and c_H, as well as the volume V_H, for the phases $Pb_{3-2x}K_xNd_x(PO_4)_2$ with x-values of 0.20, 0.25, 0.50, and 0.75. As x increases, a_H experiences a very slight decrease, whereas c_H undergoes a more noticeable increase. The volume V_H shows a subtle decrease overall.

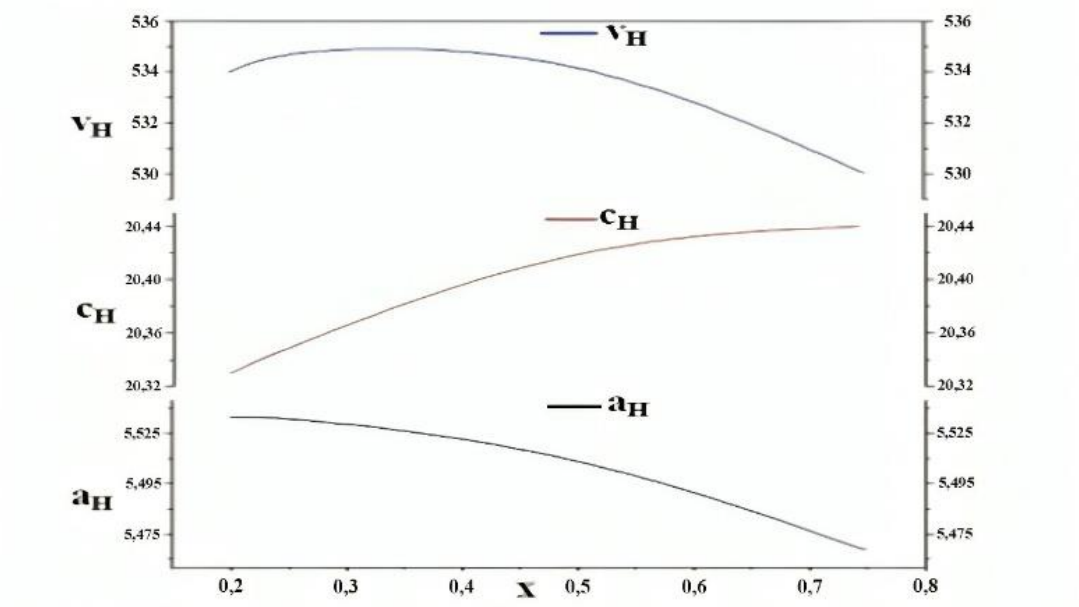

Figure 1. The variations in the parameters a_H and c_H, as well as the volume V_H, for the solid solutions $Pb_{3-2x}K_xNd_x(PO_4)_2$ with x values of 0.20, 0.25, 0.50, and 0.75.

The change in a_H becomes more pronounced as x exceeds 0.50, while the variation in cH remains relatively small. This decrease in volume, which is due to the substitution of Pb^{2+} by K^+ and Nd^{3+}, aligns well with the values of the ionic radii of these cations. Specifically, the average ion radius of K^+ and Nd^{3+} is 1.32 Å, slightly smaller than that of Pb^{2+} at 1.33 Å. The ionic radii are as follows: rK^+ = 1.55 Å and rNd^{3+} = 1.09 Å.

3.2. Isotype phases of $\beta Pb_3(PO_4)_2$.

The solid solutions $Pb_{3-2x}K_xNd_x(PO_4)_2$ for x-values of 0.05, 0.10, and 0.15 were successfully indexed in the monoclinic system, and they share structural similarities with β $Pb_3(PO_4)_2$. Table 2 provides the values for various parameters, including am, bm, cm, β, and the volume (Vm) of their elementary unit cells. These values are also compared with the corresponding parameters for the β $Pb_3(PO_4)_2$ phase for reference.

Table 2. Main crystallographic data for the solid solutions $Pb_{3-2x}K_xNd_x(PO_4)_2$ for x = 0.05; 0.10 and 0.15 [28].

X	Phase	(a_m ± 0,01)Å	(b_m± ,01)Å	(c_m ± 0,01)Å	(β± 0,01)°	(V_m ± 4)Å^3
0	$Pb_3(PO_4)_2$	13,82	5,69	9,43	102,36	724
0,05	$Pb_{2,90}K_{0,05}Nd_{0,05}PO_4)_2$	13,82	5,66	9,44	102,54	721
0,10	$Pb_{2,80}K_{0,10}Nd_{0,10}(PO_4)_2$	13,86	5,63	9,47	102,70	722
0,15	$Pb_{2,70}K_{0,15}Nd_{0,15}(PO_4)_2$	13,88	5,56	9,52	102,81	716

As x increases, there is a slight increment in the values of am, cm, and β, accompanied by a decrease in bm. Consequently, the volume experiences a subtle reduction with increasing x, consistent with the ionic radii of potassium (K^+), neodymium (Nd^{3+}), and lead (Pb^{2+}). This structural adjustment results in the phases $Pb_{3-2x}K_xNd_x(PO_4)_2$ for x = 0.05, 0.10, and 0.15 being analogous to β $Pb_3(PO_4)_2$, while those for x = 0.20, 0.25, 0.50, and 0.75 resemble α $Pb_3(PO_4)_2$. Remarkably, the transition from β $Pb_3(PO_4)_2$ to α $Pb_3(PO_4)_2$, typically requiring a temperature increase to 200°C, becomes achievable by substituting potassium (K^+) and neodymium (Nd^{3+}) ions for lead (Pb^{2+}) ions, especially starting around x = 0.20.

Figures 2, 3, and 4 illustrate the changes in parameters and volume with respect to the variable x.

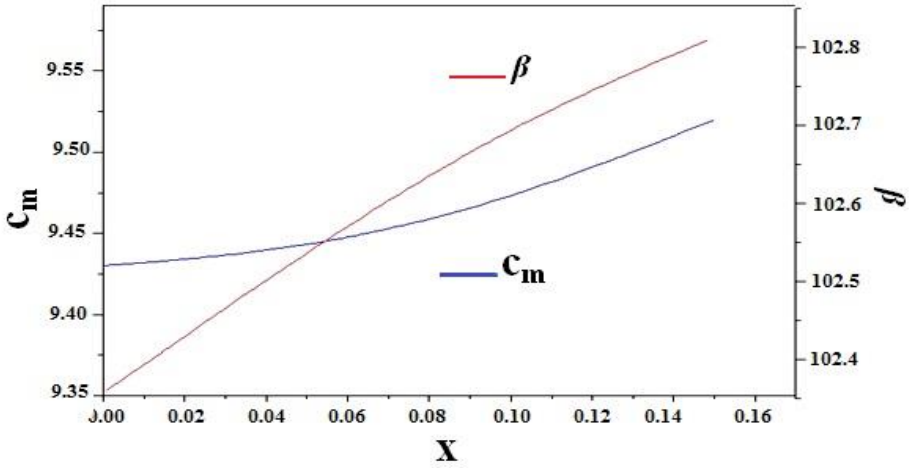

Figure 2. The evolution of the parameters Cm et β of the solid solutions$Pb_{3-2x}K_xNd_x(PO_4)_2$ For x = 0,05; 0,10 and 0,15 as a function of x.

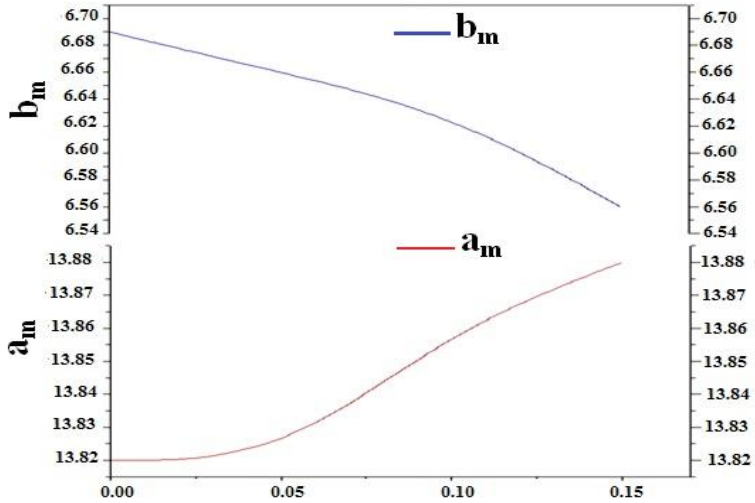

Figure 3. Volume the evolution of the parameters am et bm of the solid solutions$Pb_{3-2x}K_xNd_x(PO_4)_2$ For x = 0,05; 0,10 and 0,15 as a function of x.

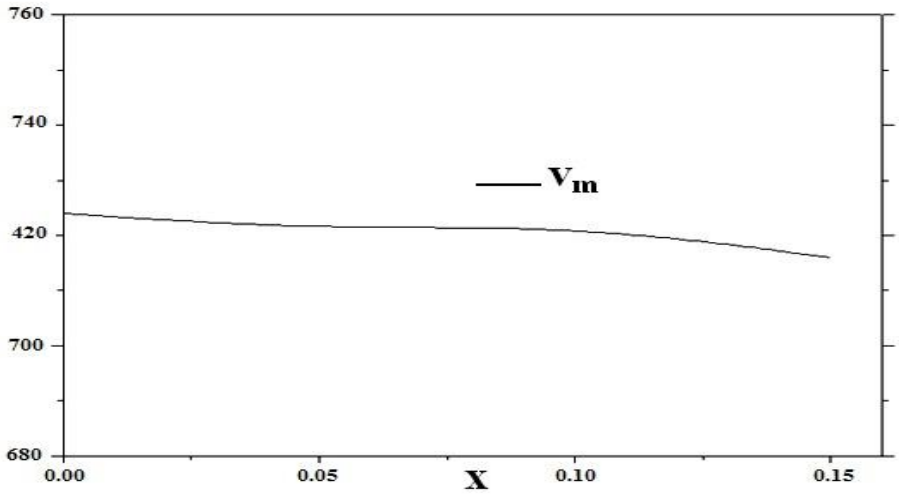

Figure 4. Volume change (Vm) of the solid solutions $Pb_{3-2x}K_xNd_x(PO_4)_2$ for x-values of 0.05, 0.10, and 0.15 as a function of x.

The phases of $Pb_{3-2x}K_xNd_x(PO_4)_2$ with x-values of 0.20, 0.25, 0.50, and 0.75 exhibit a similar structural type to $Sr_3(PO_4)_2$, which is confirmed by their X-ray diffraction patterns. Conversely, for x-values of 0.05, 0.10, and 0.15, the diffractograms indicate a structural similarity to $Pb_3(PO_4)_2$.

You can find the indexing details for the X-ray powder diffraction patterns of the new phases $Pb_{3-2x}K_xNd_x(PO_4)_2$ with x-values of 0.05, 0.10, 0.15, 0.20, 0.25, 0.50, and 0.75 in Table 3, Table 4, Table 5, Table 6, Table 7, Table 8 and Table 9.

Table 3. Indexing of the X-ray diffraction pattern for $Pb_{2,6}K_{0,2}Nd_{0,2}(PO_4)_2$.

100 I/I$_0$	d_{obs}(Å)	d_{cal}(Å)
15	4,65	4,646
<5	4,317	4,139
40	3,479	3,479
100	3,096	3,095
50	2,758	2,755
<5	2,484	2,481
<5	2,374	2,37
<5	2,328	2,323
30	2,258	2,259
10	2,165	2,16
<5	2,139	2,137
20	2,06	2,058
30	1,871	1,87
<5	1,799	1,796
15	1,748	1,747
<5	1,739	1,739
<5	1,702	1,7
10	1,649	1,649
5	1,59	1,59

Table 4. Indexing of the X-ray diffraction pattern for $Pb_{2,50}K_{0,25}Nd_{0,25}(PO_4)_2$.

100 I/I$_0$	d_{obs} (Å)	d_{cal} (Å)
25	4,649	4,646
5	4,232	4,32
50	3,48	3,48
100	3,097	3,097
70	2,757	2,755
5	2,482	2,483
5	2,37	2,37
5	2,321	2,323
40	2,26	2,261
17	2,161	2,16
5	2,139	2,138
35	2,059	2,058
40	1,872	1,872
5	1,797	1,796
25	1,748	1,748
5	1,738	1,74
5	1,701	1,7
15	1,648	1,649
5	1,592	1,591

Table 5. Indexing of the X-ray diffraction pattern for $Pb_{2,0}K_{0},5Nd_{0,5}(PO_4)_2$.

100 I/I$_0$	d_{obs}(Å)	d_{cal} (Å)
20	4,644	4,639
<5	4,315	4,317
33	3,485	3,483
100	3,102	3,101
70	2,749	2,75
<5	2,488	2,488
<5	2,364	2,365
7	2,32	2,319
20	2,27	2,27

100 I/I$_0$	d$_{obs}$(Å)	d$_{cal}$ (Å)
15	2,158	2,158
5	2,139	2,139
30	2,057	2,057
25	1,877	1,877
<5	1,79	1,793
20	1,75	1,751
<5	1,746	1,742
15	1,698	1,698
8	1,647	1,647
5	1,587	1,588
5	1,55	1,551

Table 6. Indexing of the X-ray diffraction pattern for $Pb_{1,50}K_{0,75}Nd_{0,75}(PO_4)_2$.

100 I/I$_0$	d$_{obs}$ (Å)	d$_{cal}$ (Å)
24	4,605	4,607
<5	4,294	4,291
40	3,47	3,47
100	3,092	3,092
92	2,732	2,73
<5	2,484	2,484
<5	2,347	2,348
7	2,305	2,303
20	2,271	2,271
20	2,148	2,146
8	2,132	2,13
36	2,048	2,047
30	1,877	1,876
<5	1,784	1,78
20	1,747	1,746
10	1,738	1,735
5	1,688	1,687
18	1,637	1,637
10	1,578	1,576
5	1,547	1,546

Table 7. Indexing of the X-ray diffraction pattern for $Pb_{2,85}K_{0,05}Nd_{0,05}(PO_4)_2$.

100 I/I$_0$	d$_{obs}$ (Å)	d$_{cal}$ (Å)
20	4,712	4,714
15	4,608	4,607
5	4,38	4,386
<5	4,262	4,26
10	3,606	3,608
20	3,519	3,521
65	3,49	3,493
40	3,478	3,47
<5	3,313	3,318
100	3,117	3,117
65	3,056	3,056
25	2,828	2,83
85	2,752	2,75
15	2,703	2,705
5	2,57	2,568
10	2,48	2,477
5	2,41	2,411
5	2,354	2,357
<5	2,344	2,341
<5	2,307	2,304
50	2,25	2,248
15	2,193	2,193
10	2,174	2,176
5	2,141	2,141
10	2,13	2,13
30	2,076	2,076

Table 8. Indexing of the X-ray diffraction pattern for $Pb_{2,80}K_{0,10}Nd_{0,10}(PO_4)_2$.

100 I/I$_0$	d$_{obs}$ (Å)	d$_{cal}$ (Å)
15	4,7	4,703
10	4,627	4,62
<5	4,378	4,374
<5	4,28	4,277
<5	3,606	3,607
15	3,519	3,518
45	3,49	3,493
25	3,475	3,475
<5	3,315	3,316
100	3,116	3,115
50	3,069	3,068
15	2,816	2,815
55	2,756	2,753
10	2,691	2,693
< 5	2,56	2,559
5	2,402	2,404
<5	2,35	2,351
< 5	2,349	2,349
< 5	2,31	2,309
70	2,254	2,253
10	2,189	2,187
10	2,181	2,18
10	2,144	2,142
10	2,139	2,138
20	2,074	2,074

Table 9. Indexing of the X-ray diffraction pattern for $Pb_{2,70}K_{0,15}Nd_{0,15}(PO_4)_2$.

100 I/I$_0$	dobs (Å)	dcal (Å)
15	4,669	4,668
<5	4,64	4,641
5	4,348	4,346
<5	4,296	4,298
< 5	3,601	3,6
30	3,502	3,503
50	3,482	3,482
20	3,475	3,474
5	3,31	3,31
100	3,106	3,106
50	3,081	3,078
20	2,781	2,78
50	2,757	2,756
<5	2,664	2,663
5	2,539	2,533
7	2,48	2,484
<5	2,385	2,385
<5	2,362	2,362
<5	2,331	2,334
5	2,321	2,321
75	2,256	2,256
10	2,185	2,185
7	2,173	2,173
10	2,148	2,149
10	2,145	2,143
20	2,063	2,063

4. Conclusions

Our ongoing research has successfully developed innovative solid solutions labeled as $Pb_{3-2x}K_xNd_x(PO_4)_2$, with x taking values of 0.05, 0.10, 0.15, 0.20, 0.25, 0.50, and 0.75. These compounds were synthesized by substituting 2x moles of Pb^{2+} ions in $Pb_3(PO_4)_2$ with x moles of K^+ and x moles of Nd^{3+} ions.

The resulting $Pb_{3-2x}K_xNd_x(PO_4)_2$ phases exhibit structural similarities to β-$Pb_3(PO_4)_2$ for x values of 0.05, 0.10, and 0.15. For x values of 0.20, 0.25, 0.50, and 0.75, the crystal structures resemble that of $Sr_3(PO_4)_2$. This structural transition is associated with a slight volume reduction, which is consistent with the smaller ionic radii of potassium and neodymium compared to lead.

In $Pb_3(PO_4)_2$, the phase transition from monoclinic to rhombohedral occurs at 200°C. For the solid solution $Pb_{3-2x}K_xNd_x(PO_4)_2$, the rhombohedral phase is stable at room temperature when x equals or exceeds 0.20. It is anticipated that the temperature at which the monoclinic-to-rhombohedral transition occurs will progressively decrease as the lead substitution level (x) increases from 0 to 0.15. Similarly, rhombohedral phases with x values of 0.20 or higher at room temperature are expected to become monoclinic at lower temperatures as x increases.

Author Contributions

All authors have read and agreed to the published version of the manuscript.

Institutional Review Board Statement

Not applicable.

Informed Consent Statement

Not applicable.

Data Availability Statement

Data supporting the findings of this study are available upon reasonable request from the corresponding author.

Funding

This research received no external funding

Acknowledgments

Conceptualization, C.M.; methodology, S.Z. and B.G.; software, C.M. and Y.G.; validation, M.T. and B.S.; formal analysis, C.M., Y.G., M.H., and S.E.; data curation, S.Z. and B.G.; writing—original draft preparation, C.M. and Y.G.; visualization, M.H. and S.E.; supervision, M.T. and B.S.; project administration, B.S.

Conflicts of Interest

The authors declare that they have no known competing financial interests or personal relationships that could have appeared to influence the work reported in this paper.

References

1. Nejjar, R.; Rghioui, L.; EL Jouhari, N.; Benarafa, L.; Knidiri, M.; Lorriaux, A.; Wallart, F. Contribution to the structural study of acaln(po4)2 monophosphates (a = k, rb, cs; ln = rare earth) by vibration and optical probe spectroscopies . *Can. J. Anal. Sci. Spectrosc.* **2000**, *45*, 140-147.

2. Keller, L.P.; McCarthy, G.J.; Garvey, R.G. *Mater* Crystal chemistry of ABC (PO4) 2 phases (A= K, Rb, Cs; B= Ca, Sr; C= Ln and Bi) with the hexagonal LaPO4 structure. *Res. Bull*. **2000**, *20*, 459-462, https://doi.org/1016/0025-5408(85)90014-5.
3. Belhabra, M.; Zerraf, S.; Kheireddine, A.; Fahim, I.; Tridane, M.; Abouimrane, A.; Belaaouad, S. Vibrational Study, Reinvestigation of the Crystal Structure of MgHPO4.3H2O and Calculated IR Frequencies for the PO4 3- by Isotopic Substitutions. *Biointer. Res. Appl. Chem.* **2022**, *12*, 4140–4154, https://doi.org/10.33263/BRIAC123.41404154.
4. Oubouaza , R.; Benson , M.; Wojciechowski , J.; Chtita , S. ; Tridane, M.; Belaaouad, S. Synthesis, Crystal Structure, Vibrational Study and DFT Computation of Barium Dihydrogenomonophosphate Ba(H2PO4)2. *Biointer. Res. Appl. Chem.* **2022**, *12*, 1120-1133, https://doi.org/10.33263/BRIAC121.11201133.
5. Vlasse, M.; Bochu, P.; Parent, C.; Chaminade, J. P; Daoudi, A.; Le Flem, G.; Hagenmuller, P. Structure determination of calcium neodymium potassium double phosphate CaKNd (PO4) 2. *Acta Cryst.* **1982**, *B38*, 2328-2331, https://doi.org/1107/S0567740882008735.
6. Gourja, B.; Daoudi, A.; Tridane, M.; Belaaouad, S. Chemical Preparation, Crystallographic Characterization and Investigation of Ferroelectric Properties of TlCaDy $(PO_4)_2$ and TlCaNd $(PO_4)_2$. *Int. j. trend res. dev*. **2016**, *3*, 605-607.
7. Majdi, E.M.; Zerraf, S.; Ameur, S.; Mizeb, K.; Belghiti, M.E.; Zeroual, A.; Belaaouad, S. Synthesis, crystal structure, DFT studies, and Hirshfeld surface analysis of a new Strontium Polyphosphate Form α-Sr(PO3)2. *J. of S. S. Chem.* **2024**, *329*, 124306, https://doi.org/10.1016/j.jssc.2023.124306.
8. Parent, C.; Le Flem, G.; Et-Tabirou, M.; Daoudi. A. On some new green emitting phosphors with Sr3 (PO4) 2 type structure. *S. S. Commun.* **1981**, *37*, 857-862, https://doi.org/1016/0038-1098(81)90497-X.
9. Chen, F.; Yuan, X.; Zhang, F.; Wang, S. Photoluminescence properties of Sr3 (PO4) 2: Eu2+, Dy3+ double-emitting blue phosphor for white LEDs. *Opt. Mater*. **2014**, *37*, 65-69, https://doi.org/10.1016/j.optmat.2014.04.046.
10. Bleser, T.; Berge, B.; Bismayer, U.; Salje, E. K. H. The possibility that the optical second-harmonic generation in lead phosphate, Pb_3 $(PO_4)_2$, is related to structural imperfections. *J. Condens. Matter Phys*. **1994**, *6*, 2093, https://doi.org/10.1088/0953-8984/6/10/027 .
11. Brlxner, L.H.; Bierstedt, P.E.; Jaep, W.F.; Barkley, J. R. α-Pb_3 $(PO_4)_2$—A pure ferroelastic. *Mat. Res. Bull*. **1973**, *8*, 497-504, https://doi.org/1016/0025-5408(73)90125-6.
12. Bismayer , U.; Salje. E. Ferroelastic phases in Pb_3 $(PO_4)_2$–Pb_3 $(AsO_4)_2$; X-ray and optical experiments. *Acta Cryst*. **1981**, *A37*, 145-153, https://doi.org/1107/S0567739481000417.
13. Majdi, E.M.; El Makhloufy, S.; Ouasri, A.; Saadi, M.; El Ammari, L.; Belaaouad, S. Chemical preparation, crystal structure reinvestigation and vibrational study of metacarboxyphenyl ammonium dihydrogenomonophosphate (C7H4NH3OOH)H2PO4 (m-C AMP). *Mol. Cryst. And liq. Cryst.* **2021**, *714*, 14–25, https://doi.org/10.1080/15421406.2020.1848255.
14. El Makhloufy, S.; Fahim, I.; Belhabra, M.; Zerraf, S.; Belaaouad S. X-ray diffraction and vibrational data for a series of triphosphates type MIINa3P3O10. 12H2O (MII= Cu, Ni and Mg) and their anhydrous forms MIINa3P3O10. *J. Indian Chem. Soc*. **2022**, *99*, 100449, https://doi.org/1016/j.jics.2022.100449.
15. Majdi, El. M.; Zerraf, S.; Marouani, H.; El Makhloufy, S.; Belhabra, M.; Ouasri, A.; Naimi, Y.; Belaaouad, S. Structural and vibrational study of titanium Monophosphates Na0. 5M0. 25Ti2 (PO4) 3 (M= Mn, Ni). *Med. J. Chem*. **2019**, *9*, 355-362, https://doi.org/10.13171/mjc01911281083emm.
16. Majdi, E.M.; Zerraf, S.; Belhabra, M.; Belaaouad, S. Chemical preparation, crystal structure and vibrational study of MnNa3P3O10.12H2O and X-ray characterization of the new anhydrous triphosphate MnNa3P3O10. *Pha. Trans. December* **2021**, *2022*, 50-63, https://doi.org/10.1080/01411594.2021.2009478.
17. Majdi, E.M.; Tridane, M.; Zerraf, S.; Belaaouad, S. Chemical preparation, crystallographic characterization, vibrational study and thermalbehavior of a new cyclotriphosphate CaNH4P3O9H2O. *Phosphorus, Sulfur, and Silicon and the Related Elements* **2022**, *1160-1169*, https://doi.org/10.1080/10426507.2022.2065675
18. El Makhloufy, S.; Oubouaza, R.; Ouasri, A.; Belaaouad, S. X-Ray diffraction and infrared spectroscopy data review analyses of the Calcium phosphates. *Biointer. Res. Appl. Chem.* **2022**, *12*, 732–755, https://doi.org/10.33263/BRIAC121.732755.
19. Majdi, E.M.; Belhabra, M.; Ouasri, A.; Fahim, I.; Essehly, R.; Belaaouad, S. Chemical Preparation, Crystal Structure Reinvestigation and Vibrational Study of $CoNa_3P_3O_{10}.12H_2O$ and X-ray Characterization of the

New Anhydrous Triphosphate $CoNa_3P_3O_{10}$. *Biointer. Res. Appl. Chem.* **2022**, *12*, 2586–2602 https://doi.org/10.33263/BRIAC122.25862602.

20. El Makhloufy, S.; Tridane, M.; Marouani, H.; Zerraf, S.; Belhabra, M.; Cherqaoui, A.; Belaaouad, S. Chemical preparation, thermal behavior and infrared studies of the new cyclotriphosphate tetrahydrate of manganese and distrontium, $MnSr_2$ (P_3O_9) 2.4 H_2O. *Med. J. Chem.* **2019**, *9*, 280-289, https://doi.org/10.21474/IJAR01/8432.
21. Harbi, A.; Aharbil, Y.; Moutaabbid, M.; Labrim, H.; Benyoussef, A.; Benmokhtar, S. Understanding the Magnetic, Electronic and Optical Properties of Iron Titanium Oxyphosphate Fe0. 5TiOPO4 Using DFT, GGA and GGA+ U Approaches. Jour. of App. Surf. and Inter. 2018, 3 (1–3), 17–21 . https://doi.org/10.48442/IMIST.PRSM/jasi-v3i1-3.11244.
22. Oubouaza, R.; Marouani, H.; Zerraf, S.; Belhabra, M.; Ouasri, A.; Tridane, M.; Belaaouad, S. Chemical preparations, crystal data for monophosphates and condensed phosphates associated to strontium and IR studies of their anions. *Int. J. of Emer. Tr. in Eng. Res. (IJETER).* **2020**, *8*, 6587-6598, https://doi.org/10.30534/ijeter/2020/265892020.
23. Lakhlifi, H.; Moutataouia, M.; Moukhfi, C.; Benchikhi, M.; Er-Rakho, L.; Guillemet-Fritsch, S.; El Ouatib, R. Sol-Gel Synthesis and Properties of Novel Inorganic Chromophore Based on Tetrahedral Coordination of Cu2+ in A (1-x) CuxMoO4:(A= Co, Mn). Inorg. Chem. Com. 2023, 158, 111590. https://doi.org/10.1016/j.inoche.2023.111590.
24. Marouani, H.; Oubouaza, R.; Zerraf, S.; Ouasri, A.; Tridane, M.; Belaaouad, S. Chemical preparations, crystal data for monophosphates and condensed Phosphates associated to manganese and IR studies of their anions. *Int. J. of Emer. Tr. in Eng. Res (IJETER).* **2020**, *8*, 4784-4798, https://doi.org/10.30534/ijeter/2020/116882020.
25. Majdi, E.M.; Tridane, M.; Zerraf, S.; Belaaouad, S. Chemical Preparations and X-ray Diffraction Data of Cyclotriphosphates Type $MnMII_2(P_3O_9)_2.nH_2O$ with MII Alkaline Earths. *Biointer. Res. Appl. Chem*. **2022**, *12*, 6021–6031, https://doi.org/10.33263/BRIAC125.60216031.
26. El Makhloufy. S.; Majdi, E.M.; Ouasri, A.; Chtita, S.; Saadi, M.; El Ammari, L.; Cherqaoui, A.; Belaaouad, S. Synthesis, crystal structure, IR, Raman-spectroscopy and DFT computation of monostrontium phosphate monohydrate, Sr $(H_2PO_4)_2\cdot$ H_2O. *J. Coord. Chem.* **2020**, 73, 2328-2346, https://doi.org/10.1080/00958972.2020.1815014.
27. Majdi, E.M.; El Makhloufy, S.; Chtita, S.; Belaaouad, S. Synthesis, crystal structure, IR, Raman spectroscopy, and DFT computation of metacarboxyphenyl ammonium dihydrogenomonophosphate ($C_7H_4NH_3OOH$) H_2PO_4(m-C AMP*). Inorg. and Nan. Met. Chem.* **2021**, *52*, 633-642, https://doi.org/10.1080/24701556.2021.1946081.
28. Zerraf, S.; Tridane, M.; Belaaouad, S. Crystal structure, vibrational and spectroscopic study of single crystal ($C_6H_{15}N_4O_2$) H_2PO_4. H_2O. *Mor. J. Chem.* **2020**, *8*, 428-438, https://doi.org/10.48317/IMIST.PRSM/morjchem-v8i2.16988.

Publisher's Note & Disclaimer